

Transpolar observations of the morphological properties of Arctic sea ice

Donald K. Perovich,¹ Thomas C. Grenfell,² Bonnie Light,³ Bruce C. Elder,¹ Jeremy Harbeck,⁴ Christopher Polashenski,⁵ Walter B. Tucker III,⁶ and Casey Stelmach⁵

Received 28 April 2008; revised 22 August 2008; accepted 13 November 2008; published 30 January 2009.

[1] During the 5 August to 30 September 2005 *Healy Oden* Trans-Arctic Expedition a trans-Arctic survey of the physical properties of the polar ice pack was conducted. The observational program consisted of four broad classes of snow and ice characterization activities: observations made while the ship was in transit, ice station measurements, helicopter survey flights, and the deployment of autonomous ice mass balance buoys. Ice conditions, including ice thicknesses, classes, and concentrations of primary, secondary, and tertiary categories were reported at 2-hour intervals. Pond fractions were large early in the cruise at the southern edge of the ice pack, reaching peak values of 0.5 and averaging 0.25. Ice concentrations ranged from 0.8 to 1.0 north of 79°N, save for an area between 88°30'N and 89°30'N, where polynyas and thin ice were observed. Surveys of snow depth, ice thickness, and ice properties were conducted at ice stations. Thickness observations suggest a general latitudinal trend of increasing ice thickness moving northward, with considerable variability from floe to floe and within a single floe. Average floe thicknesses varied from 1.0 to >2.8 m, and the standard deviation of thickness on an individual floe was as large as 1 m. Ice crystallography showed a large amount of granular ice. The average optical-equivalent soot content was 4 ng C g⁻¹ for new snow, 8 ng C g⁻¹ for the surface granular layer of multiyear ice, and 18 ng C g⁻¹ for the interior of multiyear ice, indicating a tendency of the particulates to concentrate at the surface with melting.

Citation: Perovich, D. K., T. C. Grenfell, B. Light, B. C. Elder, J. Harbeck, C. Polashenski, W. B. Tucker III, and C. Stelmach (2009), Transpolar observations of the morphological properties of Arctic sea ice, *J. Geophys. Res.*, *114*, C00A04, doi:10.1029/2008JC004892.

1. Introduction

[2] General circulation model results indicate that changes in the sea ice cover are both an indicator and a potential amplifier of climate change [Rind *et al.*, 1995]. Satellite observations offer substantial evidence of a reduction in the areal extent of Arctic sea ice [Johannessen *et al.*, 1995; Cavalieri *et al.*, 1997; Parkinson *et al.*, 1999; Comiso, 2002; Stroeve *et al.*, 2005; Serreze *et al.*, 2007; Stroeve *et al.*, 2007] and perennial ice fraction [Rigor and Wallace,

2004; Nghiem *et al.*, 2006; Kwok, 2007; Comiso *et al.*, 2008; Nghiem *et al.*, 2007] over the past decades. Record minimum ice extents were observed in September 1998, and again in 2002, 2005, and 2007. Comparison of submarine sonar data collected in the 1990s to similar data from the 1960s and 70s indicates that mean ice drafts in the Central Arctic have decreased an average of 40% during the period [Rothrock *et al.*, 1999]. In addition, the ice thickness distribution in sonar data from the Beaufort Sea [Tucker *et al.*, 2001] shows fewer thick multiyear ice floes after 1987.

[3] Remote sensing results provide powerful tools to assess the state of the Arctic sea ice cover. In situ ice observations are complementary, providing information that is difficult or impossible to obtain remotely. This includes high spatial resolution measurements of snow depth and ice thickness, as well as information on melt pond characteristics and ice structure. Ice thickness, extent, and concentration are indicators of climate change. Ice surface conditions, melt pond fractions, and the amount of open water directly impact the ice albedo feedback; a potential amplifier of climate change.

¹CRREL, ERDC, Hanover, New Hampshire, USA.

²Department of Atmospheric Sciences, University of Washington, Seattle, Washington, USA.

³Polar Science Center, University of Washington, Seattle, Washington, USA.

⁴Geophysical Institute, University of Alaska Fairbanks, Fairbanks, Alaska, USA.

⁵Thayer School of Engineering, Dartmouth College, Hanover, New Hampshire, USA.

⁶Terry Tucker Research, Enfield, New Hampshire, USA.

[4] There have been other surface-based efforts to characterize the ice cover in the Marginal Ice Zone [Tucker *et al.*, 1987]; in the Siberian Arctic [Haas and Eicken, 2001]; the transpolar drift region [Haas, 2004]; and across the Arctic Basin [Tucker *et al.*, 1999]. The *Healy Oden* Trans-Arctic Expedition 2005 (HOTRAX 2005) afforded a rare opportunity to make surface-based measurements describing the morphological properties and spatial variability of the summer sea ice cover sampled across the Arctic Basin [Darby *et al.*, 2005]. In this paper we present surface-based observations of snow depth, ice thickness, ice concentration, pond fraction, and multiyear ice fraction. In addition, information on ice surface conditions and internal properties is reported. A similar cruise, the 1994 Arctic Ocean Section (AOS94), yielded a wealth of information about the properties and spatial variability of the Arctic atmosphere, ice, ocean, and biosphere under environmental conditions typical of a decade ago [Tucker and Cate, 1996; Tucker *et al.*, 1999]. Results from HOTRAX 05 provide an update and a comparison for the AOS94 data as well as a benchmark for future changes in the mass balance of the Arctic sea ice.

2. Instruments and Methods

[5] Four broad classes of snow and ice morphology studies were carried out during HOTRAX: observations made while the ship was in transit; measurements made at ice stations; helicopter photography flights, and the installation of 3 autonomous ice mass balance buoys. The centerpiece of the in-transit measurements was an ice watch, where ice conditions were reported every 2 hours while the ship was in transit. The Antarctic Sea ice Processes and Climate (ASPeCT) protocol [Worby, 1999] was used and the ice thickness, concentration, and type were recorded for the primary, secondary, and tertiary ice types encountered. For this cruise first year ice was ice that formed during the 2004–2005 growth season. First year ice was delineated from multiyear primarily on the basis of surface topography, but also from ice thickness and salinity. Fractional areas of melt ponds, sediment laden ice, and biologically rich ice were estimated. Air temperature, wind speed, cloud fraction, and visibility were recorded. In addition to the ice observations, photographs were taken to help characterize the ice conditions. The compiled data set of this information provides a broad spatial overview of the properties of the ice cover across the Arctic Basin.

[6] There were 28 ice stations during the cruise where on-ice surveys of snow depth, ice thickness, and pond depth were made. Floes representative of ice conditions at each location were selected for the on-ice measurements. The surface ice surveys consisted of horizontal transects, hundreds of meters to kilometers long, where measurements were made every 5 m. The shape of the transects varied from floe to floe and were designed to effectively sample snow depth and ice thickness. Open melt ponds were avoided for safety reasons. The ponds were sampled separately. The precise survey pattern varied depending on the size and shape of the individual floe and on the amount of time available at each station. A Geonics EM-31 electromagnetic induction sensor [Haas *et al.*, 1997; Eicken *et al.*, 2001; Haas and Eicken, 2001; Haas, 2004] was used for the ice thickness survey measurements. This device determines

the ice thickness by exploiting the large conductivity difference between sea ice and the underlying seawater. The instrument transmits a primary electromagnetic field and then measures the strength of a secondary field that is induced in the seawater. The strength of the induced field is related to the distance from the instrument to the seawater and hence the ice thickness. The maximum thickness that could be measured by this device was 6 m. The instrument averages over an area approximately 1.4 times the distance from the instrument to the ocean and has a vertical resolution of a few centimeters. Holes were also drilled through the ice for direct measurements of ice thickness and to calibrate the EM-31. Thickness surveys were conducted at 23 ice stations during the cruise.

[7] Ice cores were taken at each station for more detailed analyses of the ice properties. These 10 cm diameter cores were returned to the laboratory for processing, where they were sliced in 0.05–.10 m long sections to determine vertical profiles of ice salinity and density. A YSI Model 30 salinometer with an accuracy of 0.1 parts per thousand (ppt) was used to measure the ice salinity. Uncertainties in density were $\pm 20 \text{ kg m}^{-3}$ because of difficulty in determining sample volume. Results from the bottom of the ice have a bias toward lower densities because of brine drainage when the core is removed from the ice cover. The ice crystal structure was described by making vertical thin sections from the ice cores and then photographing these sections in both transmitted natural light and between crossed polarizers. These photographs were used to classify the ice crystallography as granular, columnar, or inclined columnar on the basis of the ice grain size and orientation [Tucker *et al.*, 1987].

[8] Characterization of the physical properties of the surface scattering layer of the ice [e.g., Light *et al.*, 2008] and of the new snow were carried out routinely at all stations. The measurements consisted of a description of the presence and thickness of distinct layers; digital photographs of the grains from each layer; a determination of the characteristic grain sizes from the photographic images; measurement of light absorbing impurities; and density profiles through the snow layers at selected sites.

[9] Helicopter photographic survey flights were conducted 1–3 times per week to extend the surface-based measurements to larger scales. Flights were typically made at relatively low altitudes of 150–700 m because of the presence of low clouds during much of the summer. Hundreds to more than a thousand photographs were taken during each flight using a digital camera (Nikon D70; 3000×2000 pixel) mounted in a pod on the side of the helicopter, looking directly downward. Depending on the altitude the pixel resolution ranged from approximately 5 to 25 cm per pixel. Flight patterns varied because of conditions, but typically consisted of 3–6 legs each 5–50 km long. Aerial photographs provide a larger-scale perspective than the surface observations and still detect smaller-scale features such as small leads, ridges, and melt ponds that satellite imagery cannot resolve.

3. Results and Discussion

[10] The HOTRAX 05 cruise track of the U.S. Geodynamics Survey Committee *Healy* is displayed in Figure 1. The *Healy* entered the ice pack on 9 August 2005 at 74°N ,



Figure 1. Map showing U.S. Geodynamics Survey Committee (USCGC) *Healy* HOTRAX 05 cruise track divided into color coded weekly segments. The locations of the 30 ice stations are also plotted. The white region highlights the ice extent in September 2005. The gray line denotes the 1994 Arctic Ocean Section cruise track.

160°W and traveled in the ice until its exit on 27 September 2005 at 77°N, 9°E. The cruise started in Dutch Harbor Alaska and crossed the Bering, Chukchi, and Beaufort Seas and the Arctic Ocean reaching the North Pole on 12 September and then headed south and exited the basin through Fram Strait. The general cruise track was defined for seafloor sampling [Darby *et al.*, 2005], though ice conditions caused some modifications to be made. Depending on ice conditions, ship speeds ranged from a few knots to little progress with multiple backing and ramming. In addition to traversing

thousands of kilometers, the cruise also encompassed the seasonal transition from summer melt to fall freezeup. Panoramic photographs taken from the bridge in Figure 2 illustrate this transition. On 14 August the surface was snow free, ponds were plentiful, and leads were not freezing. This was still the case on 26 August. By 8 September, ponds had frozen, there was a light dusting of snow, and ice skims were forming in leads. Freezeup was well advanced on 19 September. Remnant ponds were snow covered and difficult to identify and lead ice was 10 to 20 cm thick. The ice



Figure 2. Panoramas of the ice cover taken from the flying bridge of the USCGC *Healy* on 14 August, 26 August, 8 September, and 19 September. Changes due to fall freezeup are evident.

thicknesses observed during the cruise were near the annual minimum. Surface melting had ceased and on the basis of earlier observations [Untersteiner, 1961; Perovich *et al.*, 2003] bottom melting was likely nearly complete.

3.1. Ice Watch

[11] Ice watch observations of ice concentration, pond fraction and thickness are plotted in Figure 3. During the first week in the ice (9–16 August), from 75°N to 78°N, ice concentrations ranged from 0.2 to 0.8, averaging 0.72. The ice here was predominantly first year, with the thickness varying between 0.5 m and 1.0 m. There was an abundance (areal fractions of 0.2–0.5) of melt ponds in this region, some of which had melted through to the ocean. At 78°N there was a shift from first year ice to multiyear ice, with bands of first year ice occasionally encountered during the east to west excursion in week 2. Once the cruise reached 79°N, multiyear ice became dominant and ice concentrations typically ranged from 0.8 to 1.0. Nilas and young ice fractions were usually between 0.1 and 0.2. However, there was a major exception from 88°25′N to 89°29′N (8 to 11 September), where for over 100 km of the cruise track there was a large area of open water, nilas, and thin young ice.

[12] The fractional area covered by ponded ice was large early in the cruise, reaching peak values of 0.5 and averaging 0.25. The largest pond fractions were observed on first year ice, where the ice was flat and featureless with very little surface topography. At higher latitudes and later dates, the areal coverage of ponds decreased. By the end of August ponds were beginning to freeze and the pond

fraction began to decrease. As freezeup continued the ponds became snow covered and it was difficult to discern what had been a pond during the melt season.

[13] The ice thicknesses in Figure 3 are estimates based primarily on blocks of undeformed ice upturned by the ship that were visible from the bridge during the ice watch. Observations suggest a general latitudinal trend of increasing ice thickness moving northward, aside from the region of open water and thin, young ice encountered between 88°25′N and 89°29′N. Average ice thicknesses increased from 1.0 m to 1.5 m to a peak of 2.0 m above 87°N (orange and green portions of cruise track in Figure 1). During the cruise the icebreaker tried to avoid the thickest ice producing some bias toward thinner ice in the ship track.

[14] An ice watch was also conducted during the 1994 Arctic Ocean Section (AOS) [Tucker *et al.*, 1999]. This expedition made a similar trans-Arctic transect during July–August 1994. Observations of ice concentration, ice thickness, and melt pond coverage for AOS and HOTRAX were compared by grouping results into 5° latitude bands (Table 1). Ice concentrations in the Western Arctic from 70 to 80°N were substantially lower during HOTRAX than AOS. Ice thicknesses observed during HOTRAX were 0.1 m to 0.3 m less than AOS. This likely does not represent a trend in thickness, rather it is a consequence of the timing of HOTRAX roughly one month later in the melt season. There was a major difference in the pond fraction between 75 and 80°N, with HOTRAX (35%) having more than twice the pond fraction as AOS (15%). We believe that this pond

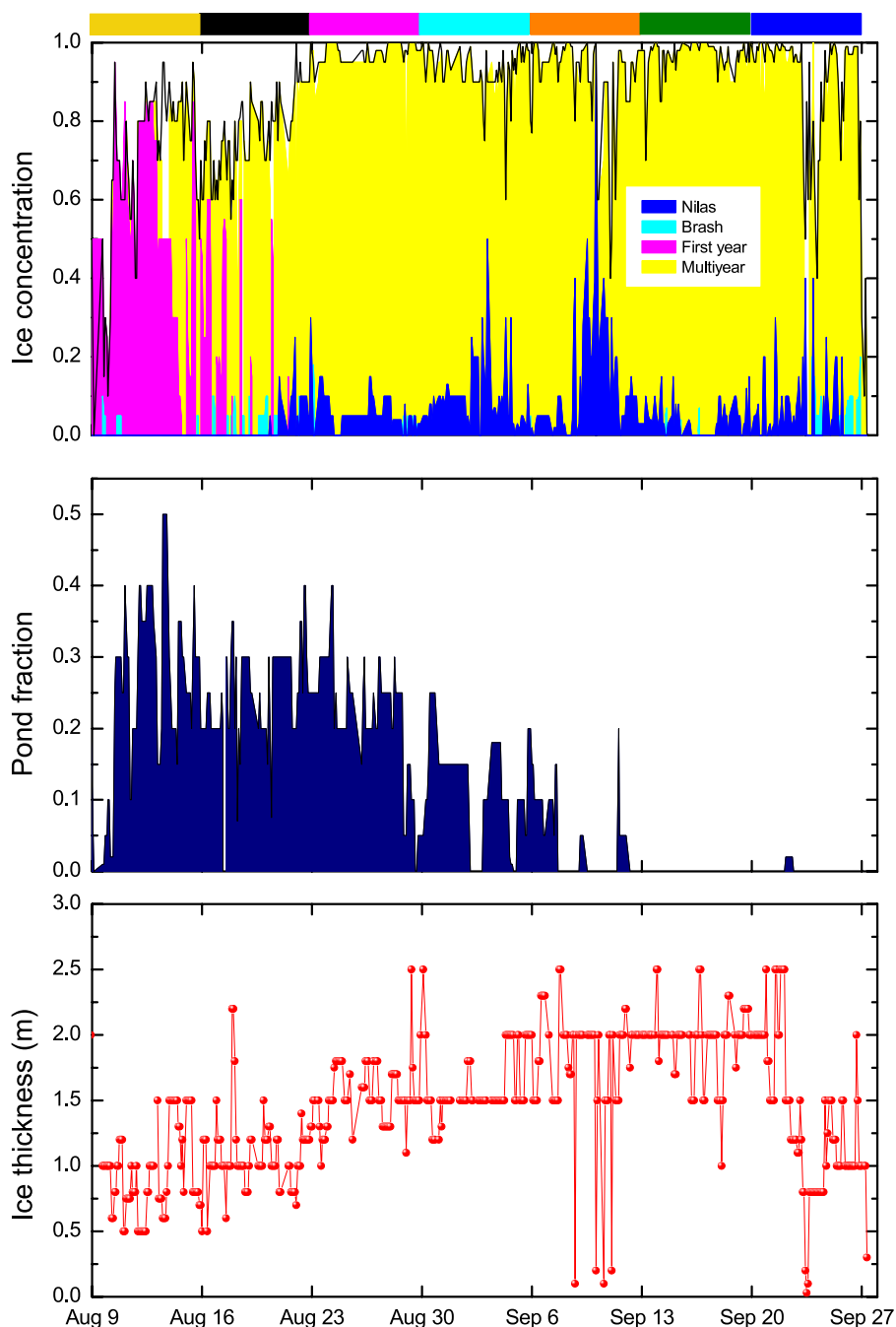


Figure 3. Results from the in-transit ice watch showing ice concentration, ice type, pond fraction, and ice thickness throughout the cruise. The color bar across the top corresponds to the drift track segments presented in Figure 1.

fraction difference was not influenced by the timing of AOS and HOTRAX, but represents a change in the ice cover.

3.2. On-Ice Observations of Snow Depth and Ice Thickness

[15] The on-ice surveys provided a more detailed examination of snow depth and ice thickness and reliable reference measurements of the snow and ice thicknesses for comparison to remotely sensed results. Statistics for the snow depth and ice thickness surveys are summarized in

Table 2. Results from six sites are presented in Figure 4 to represent the variety of conditions encountered. All of the on-ice sites were multiyear ice. Snow depth and ice thickness are plotted along the survey line (Figure 4 (top)), with Figure 4 (bottom) illustrating the top and bottom topography assuming the ice is in isostatic equilibrium. Site 4 was a flat, uniform, undeformed floe, with a mean thickness of 1.2 m and a standard deviation of only 0.03 m. The undeformed ice thickness was 1.3 m at Site 6, but the presence of a few old hummocks made the average thickness

Table 1. Comparison of in-Transit Ice Observations Made During AOS94 and HOTRAX 2005

Latitude	Ice Concentration (%)			Average Ice Thickness (m)			Fraction of Ice Area Covered by Melt Ponds (%)		
	AOS	HOTRAX	Difference	AOS	HOTRAX	Difference	AOS	HOTRAX	Difference
70–75	84	49	–35	1.1	0.9	–0.2	32	34	2
75–80	97	76	–21	1.3	1	–0.3	15	35	20
80–85	95	97	2	1.6	1.5	–0.1	16	22	6
85–90	94	91	–3	1.9	1.8	–0.1	6	6	0
90–85	94	97	3	2.2	2	–0.2	0	0	0
85–80	66	86	20	1.7	1.1	–0.6	0	0	0

equal to 1.5 m. There was no snow at Sites 4 and 6 because of ongoing summer melt. Site 13 was thicker multiyear ice, with both hummocks and ridges present resulting in an average thickness of 1.7 m. Site 16 was a multiyear floe that had a flat region surrounded by hummocks that had an average ice thickness of 1.9 m. There were regions of undeformed 1.3-m-thick ice hundreds of meters across and also large areas of deformed ice 2.3 m to 2.5 m thick. Fall freezeup was underway and the average snow depth was 0.1 m, with modest spatial variability. While the average thickness at Site 21 was comparable to Sites 13 and 16, there was much more point to point spatial variability in ice thickness. Site 27 had considerable spatial variability in both snow depth and ice thickness. Snow depths ranged from 0.01 to 0.35 m averaging 0.15 m and were correlated to topography, with deeper snow adjacent to ridge sails. While there were a few areas of relatively thin ice (0.9 m), the distinctive feature of this site was numerous ridges, a few of which exceeded 6 m in thickness.

[16] The mean, median, and standard deviation of the snow depth and ice thickness for each sampling site is plotted in Figure 5. For the first 10 sites the ice was snow free. After 30 August snow accumulated on the ice and there was a general increase in the average snow depth. This was new snow, rather than snow that survived the summer melt. A maximum average snow depth of 0.17 m was observed on 14 September on a thick, ridged floe located at 88°47'N. Average ice thicknesses showed substantial floe-to-floe variability ranging from 1 m at Site 2 to 2.8 m at Site 14. There were 5 sites (denoted by arrows in Figure 5) where more than 20% of the ice sampled had a thickness greater than 6 m. This thick ice primarily consisted of old weathered ridges. Accounting for this very thick ice would increase the average thickness at these sites by at least 1 m and for Site 28 by more than 2.5 m.

[17] All of the on-ice thickness observations (7738 individual thicknesses) were combined to generate the ice thickness distribution displayed in Figure 6. The distribution has a mean of 1.79 m, a median of 1.57 m, and a standard deviation of 0.73 m. Roughly half of the ice was between 1 and 2 m thick, with another third between 2 and 3 m. Heavily deformed ice, with thickness greater than 6 m composed about 10% of the total. No thin, young ice was measured because of the timing of the cruise at the end of the melt season. This composite picture may be biased by the tendency of the ship to travel in regions with reduced ice concentration and/or reduced ice thickness.

3.3. Surface Characteristics

[18] The structure of the surface scattering layer and the seasonal snow cover are of central interest for understanding

radiative and conductive energy exchange in the critical near-surface layers of the snow-ice system. During the melt season, the surface scattering layer is composed of individual grains of melting ice. Of particular concern are the grain sizes, which determine the volume scattering and extinction of ultraviolet, visible, infrared and microwave radiation, and bulk density, which is needed to understand heat transport. Measurements of these small-scale properties were made at each on-ice station. The sea ice cover was snow free until approximately 24 August, when the fall freezeup began. Grain sizes of both snow and melting ice were determined from 1 to 1 scale digital photographs of samples spread carefully on a ruled background making it possible to identify individual crystal sizes and shapes. The samples were handled carefully to minimize damage to the existing crystal structure. Median values of the crystal dimensions were estimated from the images by eye.

[19] For optical modeling, the small dimension is of particular interest, and values for this are shown in Figure 7a. Median and maximum dimensions are of interest for thermal and mechanical purposes, and their values are shown in Figures 7b and 7c. Values reported are essentially grain diameters or full distance across a given feature. In each case, we have separated the results into three time periods: 12–22 August, when the ice surface was bare and composed of a loose decaying granular layer (red curves), 25–31 August included the interval when new snow was deposited on the ice and the granular layer froze and hardened, and 2–20 September spanned the freezeup period with the snow depth increasing throughout the period. Thus the values quoted down to 0.45 m during this time include results from individual snow pit sites of varying depths with a maximum of 0.41 m as well as measurements in the upper 0.03 to 0.12 m of the granular layer of the underlying ice. Note the difference in abscissa scale for Figure 7c. Note the difference in scale for Figure 7c. The grain dimensions increased with depth in all cases, and were in general greatest in the bare ice layers with quite similar results in late August and September. The snow was thinner in late August and the larger values near the bottom of those profiles were also from the top of the surface scattering layer. Minimum values for bare ice ranged from 1 mm at the surface increasing to 3 mm at 0.05 to 0.06 m depth below which the ice could not be removed without damaging the crystal structure. For the snow covered cases much smaller sizes were found ranging from 0.2 mm at the surface to about 0.8 mm. Similar contrasts are apparent for the median and maximum grain sizes as well.

[20] The density profiles also show considerable variation, because of regional and temporal differences, but the

Table 2. Summary of Ice Thickness Measurements Made With the Geonics EM-31

Site	Date	Time (Alaska Daylight Time)	Latitude	Longitude	Snow Depth (cm)					Ice Thickness (cm)							
					Count	Mean	Median	SD	Minimum	Maximum	Count	%>6 m	Mean	Median	SD	Minimum	Maximum
1	12 Aug	0915–1030	76°2.119'N	157°55.807'W	209	0.0	0.0	0.0	0	0	208	0.5	153.6	120.6	68.5	97	457
2	16 Aug	0215–0400	78°26.319'N	162°26.739'W	209	0.0	0.0	0.0	0	0	209	0.0	106.2	107.7	12.7	67	172
3	18 Aug	2130–2300	78°17.493'N	176°40.739'W	134	0.0	0.0	0.0	0	0	134	0.0	120.2	123.7	24.3	64	182
4	22 Aug	2130–2300	81°13.565'N	177°11.679'W	227	3.6	4.0	3.3	0	15	227	0.0	120.0	119.3	8.3	61	142
5	25 Aug	0850–1420	83°07.844'N	174°40.283'W	450	0.0	0.0	0.0	0	0	449	0.2	164.8	149.1	52.7	8	554
6	26 Aug	0930–1050	83°17.947'N	171°53.294'W	312	0.0	0.0	0.0	0	0	312	0.0	149.4	133.3	38.9	91	317
7	26 Aug	1500–1600	83°20.028'N	171°59.351'W	132	0.0	0.0	0.0	0	0	100	24.2	247.0	212.7	100.6	70	691
8	27 Aug	0915–1050	84°18.540'N	160°38.867'W	458	0.0	0.0	0.0	0	0	416	9.2	187.0	158.5	82.4	8	726
9	28 Aug	0945–1110	84°18.6350'N	160°25.164'W	250	0.0	0.0	0.0	0	0	244	2.4	183.9	161.7	55.5	72	506
10	29 Aug	1430–1610	84°18.423'N	149°04.907'W	255	0.0	0.0	0.0	0	0	200	21.6	258.3	248.5	60.7	157	535
12	30 Aug	1300–1540	83°57.277'N	143°11.516'W	427	1.6	0.0	3.1	0	16	422	1.2	187.0	169.5	64.0	55	535
13	31 Aug	1040–1330	84°10.249'N	150°59.71'W	265	8.0	8.0	3.2	0	26	257	3.0	165.1	152.6	47.1	110	527
14	31 Aug	1900–1950	84°10.249'N	150°59.71'W	109	10.6	10.0	3.7	5	32	100	0.0	171.7	153.1	94.8	137	611
15	2 Sep	0015–0315	85°07.337'N	154°47.979'W	100	5.3	4.0	4.1	1	32	100	0.0	171.7	153.1	46.6	110	359
16	2 Sep	2230–0130	85°58.992'N	162°13.885'W	205	10.0	9.0	3.3	3	20	203	1.0	187.8	191.6	40.2	122	292
17	6 Sep	1300–1500	87°37.205'N	155°52.531'E	255	10.8	10.0	5.7	1	45	246	3.5	185.8	157.2	74.3	73	535
18	6 Sep	2100–2200	87°39.610'N	150°54.091'E	227	8.7	9.0	5.7	2	46	225	0.9	141.0	135.8	49.9	62	363
19	9 Sep	0630–0830	88°27.337'N	146°31.937'E	275	11.6	10.0	5.9	2	34	266	3.3	168.8	147.0	65.2	98	479
20	10 Sep	0100–0300	88°43.065'N	170°09.170'E	235	9.2	8.0	7.0	0	41	203	13.6	224.3	202.1	91.6	99	547
21	10 Sep	0900–1100	88°48.801'N	164°08.136'E	430	7.4	6.0	5.3	0	46	420	2.3	173.6	164.1	52.3	89	575
22	11 Sep	1820–1930	89°28.89'N	169°47.9'E	235	12.4	12.0	6.7	2	36	201	14.5	195.2	171.2	77.6	98	548
23	12 Sep	1000–1100	90°N	0°E	222	12.2	11.0	6.4	2	47	217	2.3	164.4	137.6	66.0	101	536
24	13 Sep	1930–2045	89°05.3' W	89°05.3' W	242	16.0	15.0	8.9	0	53	187	22.7	230.9	218.8	96.0	90	489
25	14 Sep	1940–2120	88°46.932'N	75°6.2'E	241	17.4	17.0	6.0	0	40	236	2.1	183.2	173.4	52.2	96	426
26	15 Sep	1910–2050	88°03.333'N	58°44.9'E	426	16.8	16.0	7.1	1	53	293	31.2	230.7	198.6	102.3	104	686
27	17 Sep	0330–0500	87°28.301'N	57°35.3'E	368	14.8	15.0	4.9	1	32	362	1.6	164.4	150.4	58.9	93	463
28	18 Sep	1645–1830	86°39.394'N	55°37.1'E	409	16.6	15.0	8.8	0	53	161	60.6	201.9	150.9	109.5	62	610
29	20 Sep	0430–0600	85°56.25'N	48°20.1'E	431	12.5	12.0	4.6	0	36	429	0.5	159.1	155.9	23.3	100	328
					7738						7030	9.1					

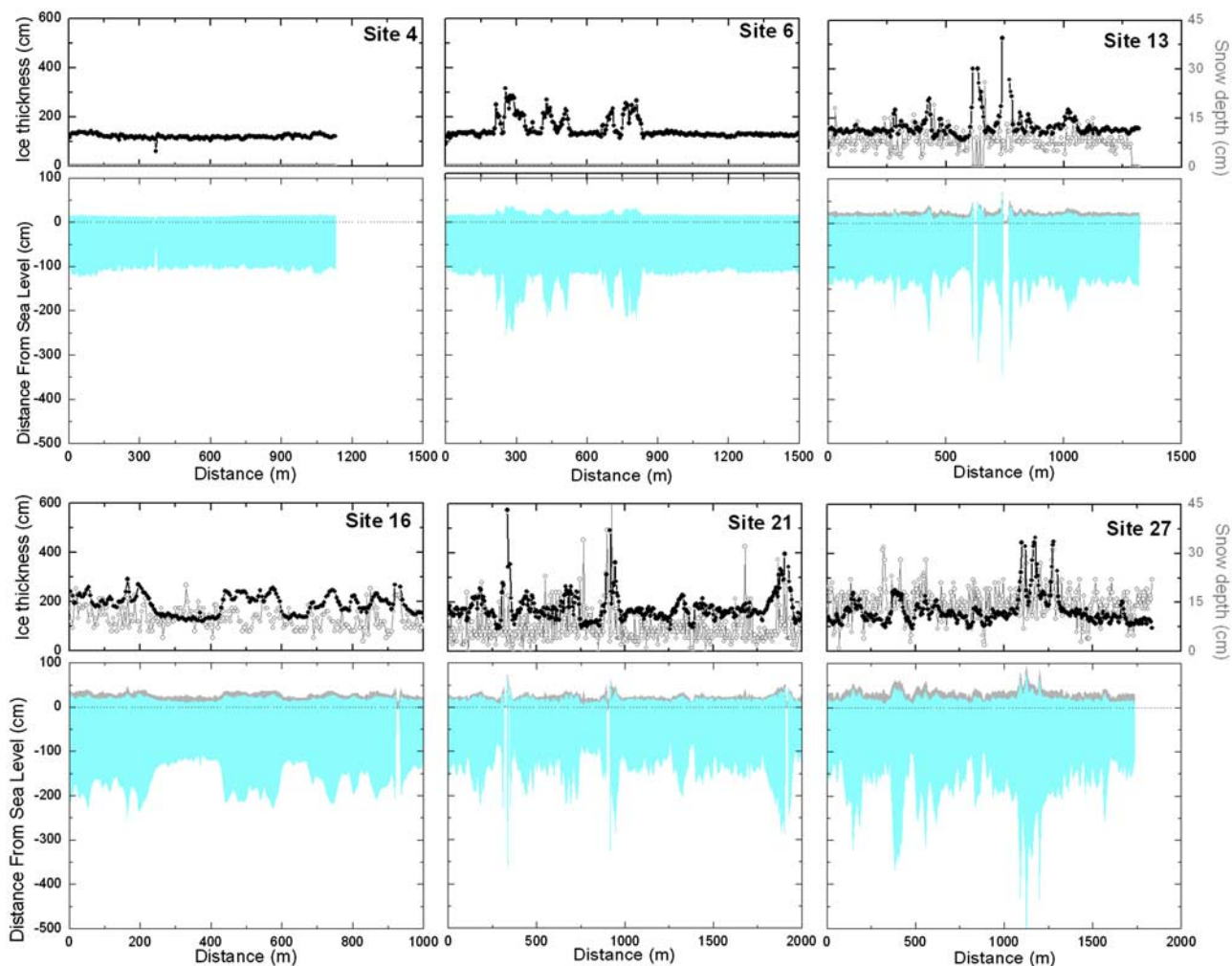


Figure 4. Results from the on-ice surveys of snow depth and ice thickness. Snow depths were measured by probing, and ice thicknesses were determined using a Geonics EM-31 electromagnetic induction sensor. At each site 3–6 holes were drilled through the ice to calibrate the electromagnetic induction sensor.

median value is near 300 kg m^{-3} in the bulk of the snowpack increasing to an arbitrary limit of 600 kg m^{-3} in the consolidated surface granular layer. On 17 September we encountered a solid ice layer due to rainfall at a depth of 0.14–0.15 m with a density of approximately 900 kg m^{-3} . In September, the density was not measured over the full range of depth quoted for grain size because the cutter could not obtain reliable values in the lower layers, which consisted of thin hard ice layers, delicate depth hoar, and frozen granular ice.

3.4. Absorbing Impurities in the Near-Surface Layers

[21] To investigate the amount of light absorbing impurities in the near-surface layers, we carried out observations of the equivalent black carbon (soot) loading of the upper 10–30 cm of the snow and ice using the filtration method used in several polar surveys [Clarke and Noone, 1985; Warren and Clarke, 1990; Grenfell et al., 2002]. Bulk samples were obtained at 23 ice stations upwind of the ship from 2 to 4 vertical layers, depending on the depth of the snow and the thickness of the surface decomposed layer.

The samples were collected in clean glass containers and returned to the ship where they were rapidly melted in a microwave oven and immediately drawn through 0.4 micron nuclepore[®] filters using a custom-built vacuum filtration system with a hand-operated vacuum pump. The volume of the meltwater was logged, and the filters were air-dried. Determination of the equivalent soot concentration, C , was performed onboard the ship by comparing the sample filters with a set of standard filters with precisely known black Carbon loading. An important advantage of this optical-based technique is that the results make it possible to compute an accurate reduction of the albedo of the snow or ice without having to specify the precise concentration or the size distribution of the impurities.

[22] In the present sample set, soot and sedimentary material were the dominant contaminants present. Samples were taken from the new snow, from the surface granular layer and from selected ice cores. The values of C showed no significant spatial trend for a given sample type. Figure 8 shows the histogram for all samples. The peak of the distribution function for concentration was about 4 ng C g^{-1}

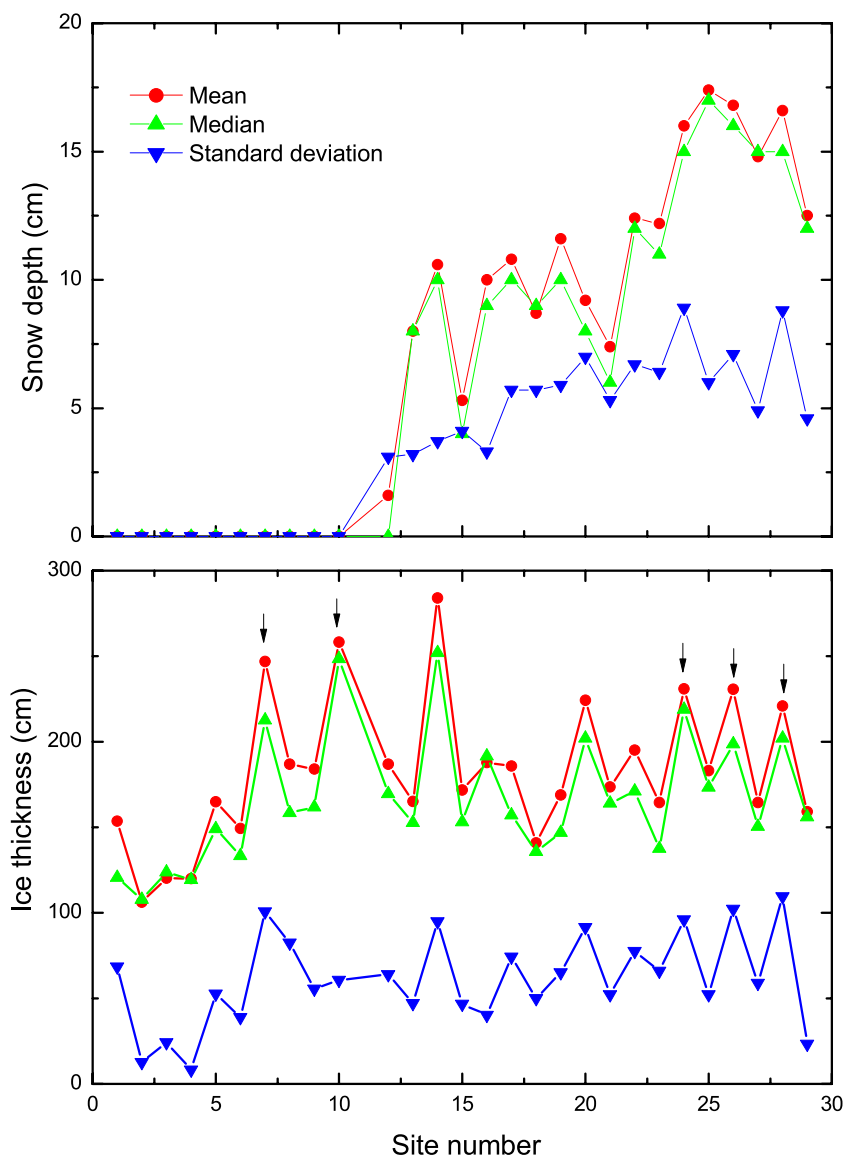


Figure 5. Mean, median, and standard deviation of (a) snow depth and (b) ice thickness from each thickness survey site. The arrows denote sites where more than 20% of the ice sampled had a thickness greater than 6 m.

(ppb by mass), which was also the average value for the snow layers. The median value was 7 ng C g^{-1} . The average concentration value was lowest for the snow covered surfaces (4 ng C g^{-1}), intermediate for the surface granular sites (8 ng C g^{-1}), and highest for the interior ice samples (18 ng C g^{-1}).

[23] On the basis of the color of the exposed filters (gray for pure soot and dark brown for sediment), we conclude that the elevated C values for the interior ice were due to the presence of marine sediments entrained in the ice. Sedimentary material was identified by its brownish color and by the presence of particles visible using a magnifying glass. Soot particles are submicron in size and are only visible under much higher magnification.

[24] The decrease in snow albedo is calculated from the soot loading and the snow grain radius. According to the

studies of *Warren and Wiscombe* [1980], for a snow grain radius of 100 microns, representative of the new snow, 4 ng C g^{-1} would reduce the albedo at 470 nm by 0.005, a level that is approximately at the limit of detectability for precise surface-based spectral albedo observations and well below the present limits for satellite observations. In the surface scattering layer, where the average value of C was about 7 ng C g^{-1} and the grain radius was typically 1 mm, the albedo decrease would be 0.02. The largest C value of 65 ng C g^{-1} would produce a corresponding decrease in visible albedo of about 0.035. Observations of ice areas with considerably higher loadings and lower albedos were encountered on the traverse, but these areas were very inhomogeneous and the present filtration technique is not suitable for such heavy sediment concentrations.

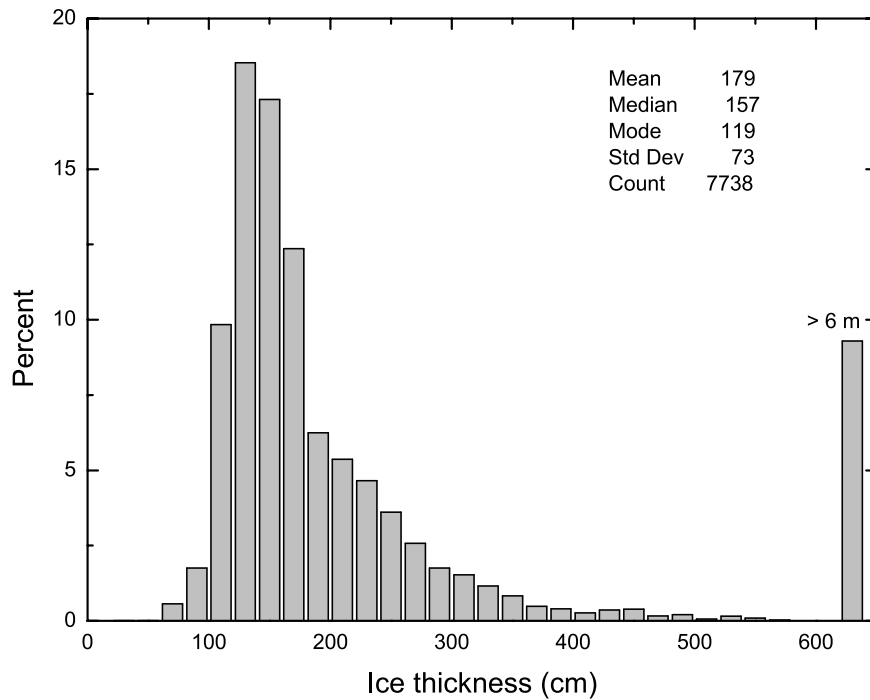


Figure 6. Ice thickness distribution combining results from all on-ice thickness measurements.

[25] The values of C observed in the surface granular layers were higher than in the new snow, even after the full summer melt, suggesting that the contaminants are concentrated at the surface as the snow melts. This is consistent with recent observations in Greenland (S. G. Warren, personal communication, 2008).

3.5. Ice Physical Properties

[26] A dozen ice cores spanning stations from across the basin were processed for physical and structural properties. Example results from a core taken in bare ice at Site 10, a thick multiyear floe at $84^{\circ}18'N$, $149^{\circ}5'W$, are presented in Figure 9. The portion of the ice above freeboard (top 0.3 m) was drained white ice, with a density of only 700–800 kg

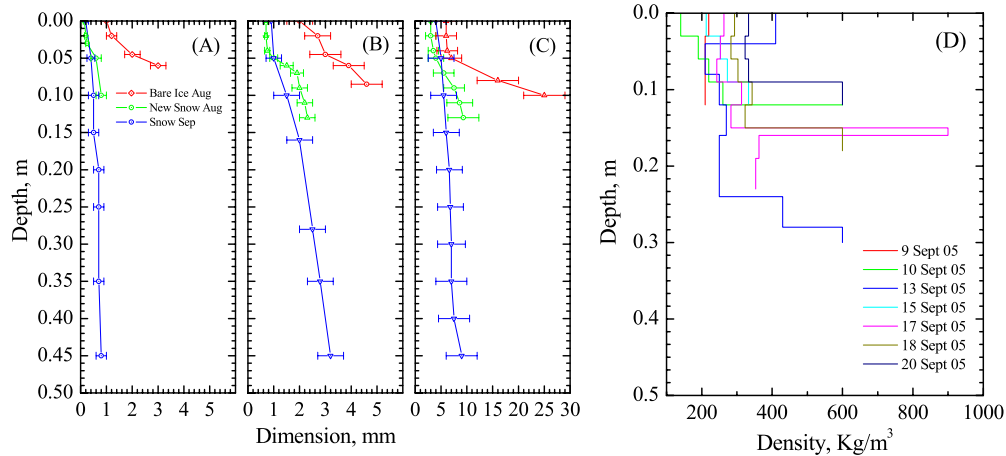


Figure 7. Grain size profiles of the surface layers including windpack, depth hoar and/or the upper part of the near-surface granular layer, and density profiles of the recently deposited snow. (a) Median of small dimension with standard deviation. (b) Median value of median grain dimension. (c) Median value of maximum grain dimension. (d) Snow density profiles at individual snow pit sites. A density of 600 kg m^{-3} was assumed arbitrarily for the consolidated surface granular layer where the scoop sampler no longer worked. The density of 900 kg m^{-3} on 17 September was for an ice layer within the snow. Red curves denote the period of bare melting ice from 12 to 22 August. The green curves include the new snow during the interval 25–31 August. The blue curves include all observations from 1 to 20 September.

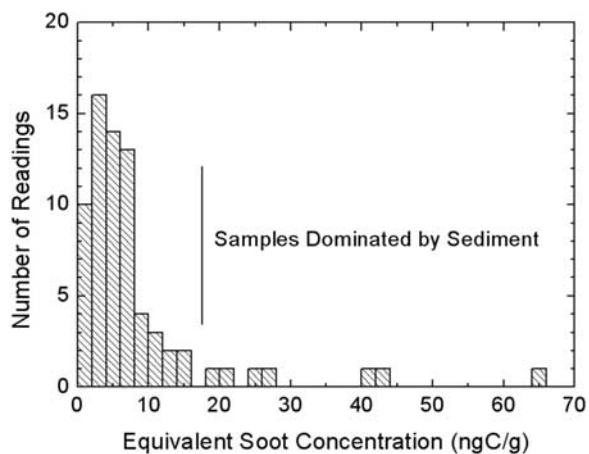


Figure 8. Histogram of the observations of equivalent soot concentration, C . The most frequent value of C was at 4 ng C g^{-1} with a median value of 7 ng C g^{-1} . All samples with values of 18 ng C g^{-1} and above were from ice cores and were dominated by sediment.

m^3 and a salinity less than 1 ppt. Deeper in the ice densities ranged from 850 to 910 kg m^{-3} and salinities were between 1 and 2 ppt. The drained top 0.3 m was highly scattering, appeared white, and consisted of granular ice (photographs in Figure 9). Below the surface layer the ice was predominantly columnar, with one narrow band of granular ice. Overall this core was 28% granular and 72% columnar.

[27] Results for all the cores are summarized in Table 3. The average bulk salinity of all the cores was 1.6 ppt and values for individual cores ranged from 1.0 to 2.2 ppt. The crystallographic structure of the cores varied greatly. For example, the granular ice fraction was 6% at Site 6 and 100% at Site 13. Five of the 12 cores were more than 50% granular, an exceptionally large portion for multiyear Arctic sea ice.

[28] Ice core results from HOTRAX are compared to other studies in Table 4. Particularly appropriate is a comparison to the 1994 Arctic Ocean Section (AOS) [Tucker *et al.*, 1999]. The ice sampled in the HOTRAX cores was generally thinner than those from AOS [Tucker *et al.*, 1999], though the sample size is small and the average 0.2 m difference could be due to additional late season

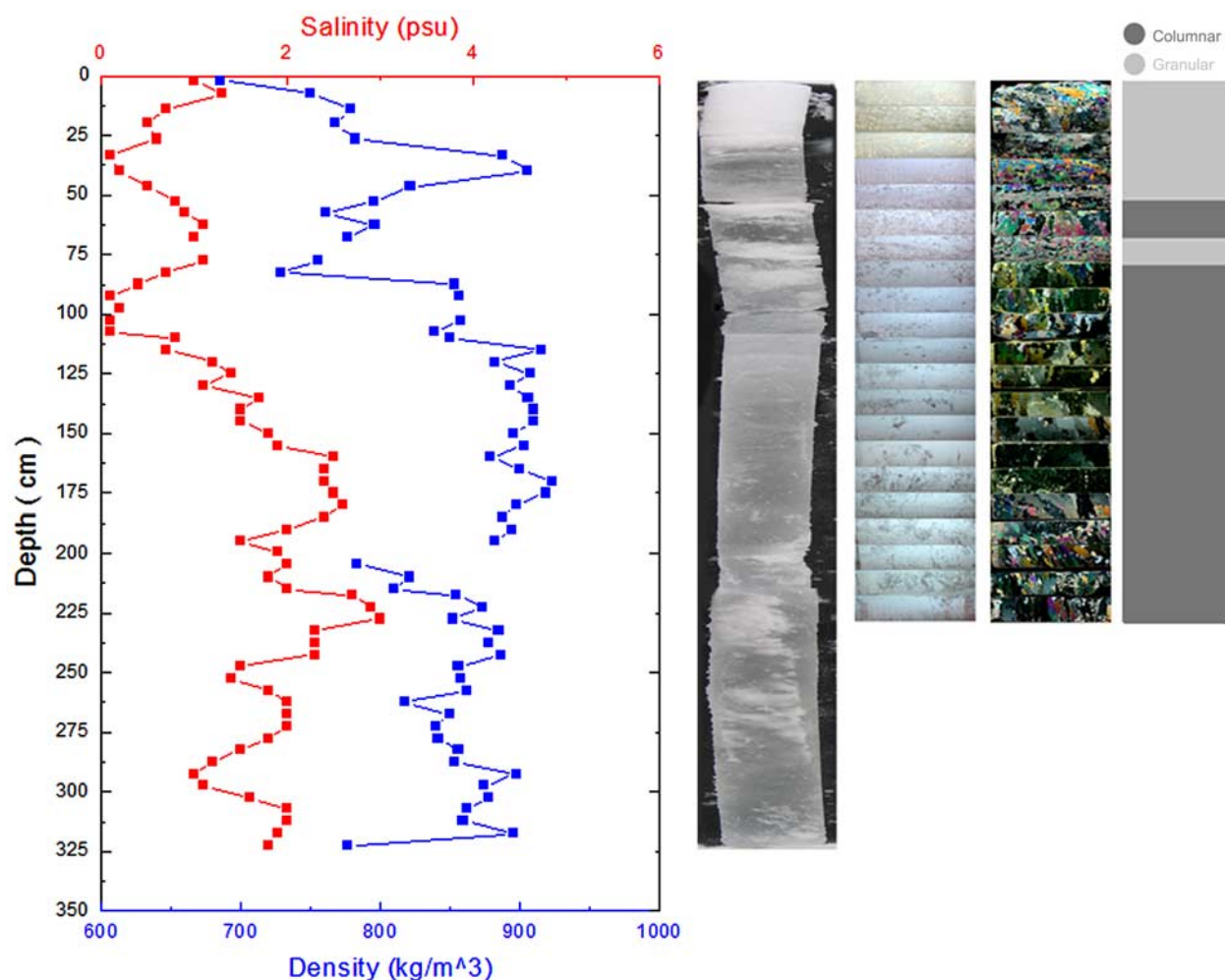


Figure 9. Ice core results from Site 10 taken on 26 August 2005. (right) The entire core, thin sections photographed under transmitted natural light, and thin sections photographed under cross polaroid filters. There were thin section photographs for only the top 225 cm of the core. (left) Vertical profiles of ice salinity and density.

Table 3. Summary of Ice Core Results^a

Date	Site	Latitude	Longitude	Ice Thickness (m)	Freeboard (m)	Bulk Salinity (ppt)	Ice Structural Composition (%)		
							Granular	Columnar	Inclined
16 Aug	2	78°26.319'N	162°40.739'W	1.10	0.10	1.4	33	12	55
18 Aug	3	78°17.493'N	176°40.739'W	1.35	0.20	1.8	77	6	17
22 Aug	4	81°13.565'N	177°11.679'W	1.35	0.20	2.0	24	74	2
25 Aug	6	83°07.844'N	174°40.283'W	>2.50	0.40	1.5	6	94	0
27 Aug	8	84°18.540'N	160°38.867'W	1.98	0.25	1.3	50	50	0
28 Aug	9	84°18.635'N	160°25.164'W	0.94	0.23	1.0	17	83	0
29 Aug	10	84°18.423'N	149°04.907'W	3.33	0.46	1.2	24	72	0
30 Aug	12	83°57.277'N	143°11.516'W	1.85	0.19	1.7	9	91	0
31 Aug	13	84°10.249'N	150°59.710'W	1.78	0.35	2.2	100	0	0
2 Sep	15	85°07.337'N	154°47.979'W	2.03	0.43	1.6	64	36	0
2 Sep	16	85°59.992'N	162°13.885'W	2.58	0.30	1.4	48	31	21
6 Sep	17	87°37.205'N	155°52.531'E	1.69	0.19	1.6	14	86	0
9 Sep	19	88°27.337'N	146°31.937'E	1.68	0.33	N/A	70	0	30
26 Sep	30	80°28.254'N	7°34.400'E	2.40	N/A	1.4	53	47	0

^aAll cores were multiyear ice.

ablation for the later HOTRAX cruise. Bulk salinities from HOTRAX were 0.3 ppt less than AOS values. Because cores were taken in multiyear ice near the end of the surface melt season in both cruises, it is unlikely that the difference in salinity was due to summer brine drainage. This conclusion is supported by previous observations by *Tucker et al.* [1999] who noted that multiyear sea ice did not have a strong temporal trend in salinity, because most drainage had already occurred in previous summers. Though lower in overall salt content, profiles of ice salinity with depth showed trends consistent with past observations, generally increasing with depth from near 0 at the surface to 1.75–3 ppt deeper. These maximum salinity values are small compared with maximum salinity observations of 3–4 ppt in previous measurements (Table 4).

[29] Examination of the crystalline structure showed a striking increase in granular ice fraction over the AOS observations [*Tucker et al.*, 1999]. Older observations elsewhere in the Arctic also place the granular fraction near 10% (Table 4). Our observations indicate a much higher granular ice fraction, of just over 40%. The observed increase in granular ice may indicate a shift toward greater amounts of ice growth under turbulent conditions. While the small sample size precludes sweeping conclusions, the observed change in ice structure warrants future study, and samples from the cores were taken for isotope analysis.

3.6. Melt Ponds

[30] This cruise provided an excellent opportunity to study melt ponds at locations across the Arctic Ocean as the ponds transitioned from summer melt to fall freezeup.

The August–September time frame encompassed both the period of peak pond coverage [*Perovich et al.*, 2002a] and the seasonal transition from open mature ponds to frozen snow covered ponds. Pond observations were made as part of the ice watch, the on-ice surveys, and the helicopter photography flights. Ponds came in all sizes and shapes. Aside from first year ice observed during the first week of the cruise and at Sites 1 and 2 (Figure 3) the pond measurements were for multiyear ice. Many of the ponds had overhanging ledges extending 10 to 50 cm around the perimeter. The overhangs were similar in shape, but smaller in scale to those found on ice edges by leads [*Perovich et al.*, 2003] and were caused by wave action in the ponds.

[31] On-ice measurements of melt pond properties were made at 18 sites and 39 individual ponds during the experiment. The depth of the pond water and the thickness of the underlying ice were measured. Later in the cruise the thickness of the frozen surface layer and the snow depth were also recorded. Pond water depths ranged from 0.16 to 0.51 m, averaging 0.3 m. The average thickness of the underlying ice was 0.90 m, with a range from 0.40 to 2.13 m. The surface of the ponds began to freeze by the last week of August. It was possible to walk on the ponds by 6 September and by 17 September the frozen surface layer was 0.40 m thick.

[32] Water temperatures in the ponds were generally at their salinity-determined freezing point. Salinities varied from 2 ppt to as high as 29 ppt for ponds that had a direct connection to the ocean. The connection could either be through the horizontal network of pond tributaries in the ice or vertically through the ice underlying the pond. In a few

Table 4. Comparison of HOTRAX Ice Properties to Earlier Observations

Year	Reference	Ice Thickness (m)	Bulk Salinity (ppt)	Ice Structure Composition (%)			Region Sampled	Month Measured
				Granular	Columnar	Other		
2005	This paper	1.75	1.6	41	51	8	Trans Arctic	Aug–Sep
1994	<i>Tucker et al.</i> [1999]	1.97	1.9	6	90	4	Trans Arctic	Jul–Aug
1991	<i>Eicken et al.</i> [1995]	2.86	2.1	18	65	17	Eurasian Sector	Aug–Sep
1986/7	<i>Meese</i> [1989]	2.88	2.8	11	88	0	Beaufort Sea	Apr
1984	<i>Gow and Tucker</i> [1987]	2.78	2.2	15	85	0	Fram Strait	Jun–Jul

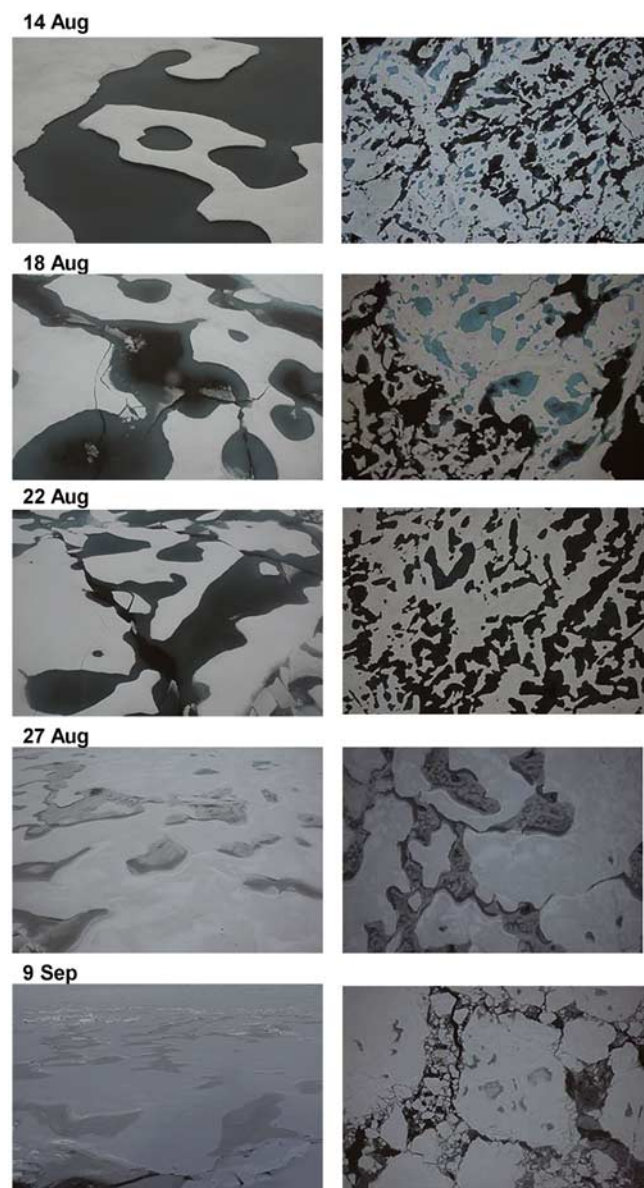


Figure 10. Time series photographs illustrating the evolution of melt ponds during freezeup. The photographs were taken (left) from the ship and (right) from a helicopter. The scale varies across Figure 10, but the ponds are typically a 1–3 m across and 5–10 m long.

cases the water in a pond was highly stratified with a fresher (12 ppt) layer on top of saltier ocean water (29 ppt).

[33] Photographs documenting the melt pond evolution are presented in Figure 10. The photographs were taken from the *Healy* (left side) and during the helicopter survey flights (right side). The mature melt ponds displayed in 14 August illustrate the complexity of pond shape and the different hues of blue associated with pond color. As the underlying ice in the pond got thinner, the pond albedo decreased and the ponds appeared darker. The very dark pond areas in the 18 August and 22 August photographs are places where the pond has melted through to the ocean. By 27 August the ponds have begun to freeze, with the shallow

ponds freezing first. By 9 September all the ponds had frozen and were covered by a layer of snow only a few centimeters thick. Snow continued to fall and drifting snow preferentially accumulated in the hollows formed by the ponds, eventually erasing the visible surface signature of the ponds. A more detailed description of the ponds can be obtained from an image analysis of the aerial photographs, as was done for 22 August. Groups of 10 individual overlapping photographs were merged into one large mosaic to increase the sample area. Using differences in brightness and color the mosaics were partitioned into three components; ice, ponds, and leads. In some cases, because of a lack of contrast, it was necessary to manually “paint” some leads or ponds to clearly delineate them. The number of pixels in each category was determined and the areal fractions of ice, ponds, and leads were calculated using Image-Pro Plus software.

[34] Figure 11 shows the areal fraction of bare ice, ponded ice, and leads determined along the flight path on 22 August. Each data point represents a mosaic of images representing an area of approximately 1.2 km². The total area of all the images processed was 55 km². The average area fractions were leads 0.07, ponds 0.29, and bare ice 0.64. Standard deviations were 0.05 for leads, 0.06 for ponds, and 0.08 for bare ice. There was a maximum point to point variability in the area fractions of about 0.2.

[35] We used these area fractions to compute large-scale estimates of albedo. The areally averaged albedo is simply

$$\bar{\alpha} = \alpha_l A_l + \alpha_p A_p + \alpha_i A_i,$$

where A is the area fraction, α is the albedo and the subscripts, l , p , i refer to leads, ponds, and bare ice respectively. The lead albedo was set to 0.07 [Pegau and Paulson, 2001] and the bare ice albedo to 0.65 [Perovich et al., 2002b]. Selecting a pond albedo is more difficult because of the variable nature of the ponds. On the basis of visual analysis of the images and previous work [Perovich et al., 2002b], a value of 0.25 was selected. The area fractions in Figure 11 were input into the above equation to compute large-scale albedos (solid line in Figure 11). Albedos for individual scenes ranged from 0.37 to 0.56 averaging 0.49. The smallest albedo occurred for the mosaic with the largest area fraction of open water (0.26) and the largest albedo was for the mosaic with the largest area fraction of bare ice (0.85).

[36] The HOTRAX area fractions and areally averaged albedos are compared to values from Surface Heat Budget of the Arctic Ocean (SHEBA) [Perovich et al., 2002a], National Technical Means [Fetterer and Untersteiner, 1998], and AOS [Perovich and Tucker, 1997] (Table 5). It was not possible to exactly match the date and position, but the comparison cases were selected so that HOTRAX was further north, later in the season, and presumably further along in the transition to fall freezeup. HOTRAX had the largest pond fraction by more than a factor of two. This large pond fraction resulted in the smallest areally averaged albedo. During SHEBA the ponds had already begun to freeze by 22 August reducing the open pond fraction to 0.02. On the same day, 7 years later, 330 km further north, the HOTRAX ponds had not yet started to freeze. The large pond fraction resulted in additional solar heat input, and

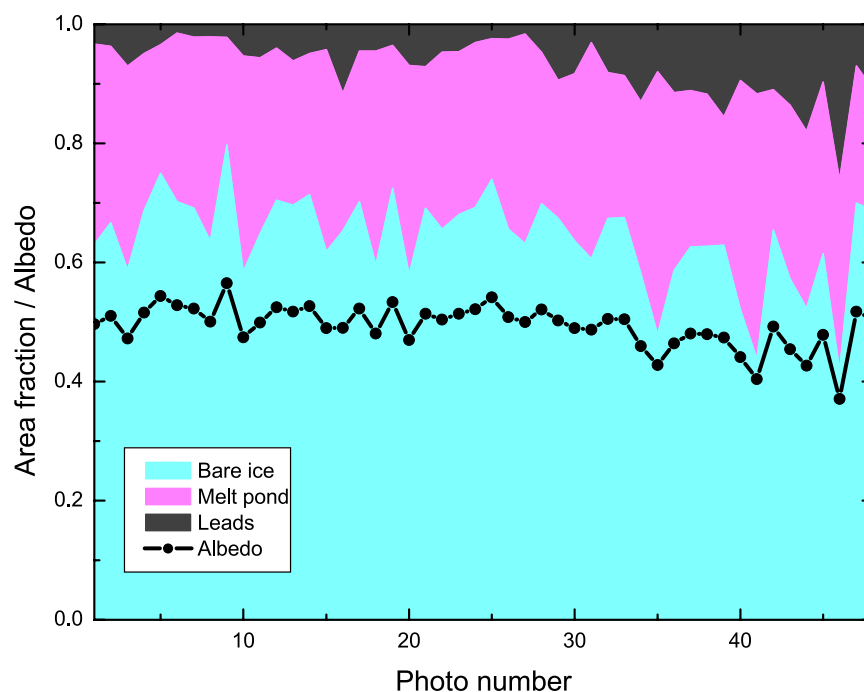


Figure 11. Analysis of aerial photographs taken on 22 August 2005 showing area fractions of bare ice, melt ponds, and leads. Each point represents an area of approximately 1.2 km².

warming, of the upper ocean [Grenfell and Perovich, 2004; Inoue *et al.*, 2008].

3.7. Autonomous Time Series Measurements

[37] By their intrinsic nature, survey cruises, such as this one, generate a series of snapshots that are best used to define the state of the ice cover and its spatial variability over a brief time period. HOTRAX was fortunate in that the two-month time period encompassed fall freezeup, a key period in the annual cycle. However, there is also great interest in the longer-term temporal evolution of the ice cover. This interest was addressed by deploying three autonomous ice mass balance buoys (IMB) during the cruise. The IMB is an autonomous, drifting buoy equipped with a data logger, satellite transmitter, barometer, acoustic rangefinders placed above the ice surface and below the ice bottom, and a thermistor string extending from the surface through the snow and ice into the upper ocean [Perovich and Richter-Menge, 2006; Richter-Menge *et al.*, 2006].

[38] Data from the buoys provided information on ice motion, snow accumulation and melt, ice growth, ice surface and bottom melt, the onset dates of melt and freezeup, and the ocean heat flux. Information from an IMB can provide important insight on the forces driving the observed changes in the ice cover. Results are presented in Figure 12 from the one buoy that lasted a full annual cycle. It was installed in the ice at 85°7.337'N, 154°47.979'W on 2 September 2005 and operated until 22 March 2007 when the ice floe melted off the coast of Greenland. The season by season buoy motion is displayed in Figure 12a. There was relatively little movement in winter and spring and more in summer and fall. Ice motion increased significantly

in fall 2006 and winter 2007 as the buoy exited out the Fram Strait and drifted down the coast of Greenland.

[39] Freezeup had already begun when the buoy was installed in 2.54-m-thick ice on 2 September 2005. It took another three and a half months until the below freezing air temperatures propagated through the ice and cold temperature pulse reached the bottom in mid-December 2005 starting new growth. There was a total ice growth of 0.48 m in winter and spring. Growth stopped in early June, but bottom melting didn't begin until the end of that month. The snowpack was shallow (0.05 m to 0.10 m) for fall and much of winter. The maximum snow depth in the first year was 0.17 in May 2006. Surface melting began on 12 June 2006 and by 3 July 2006 the snow cover had melted. Over the next 4 weeks there was 0.22 m of surface ice melt until freezeup began on 31 July. There was more snow in the second year, with 0.1 m snowfalls at the end of August and the end of September giving a peak snow depth of 0.28 m. Melting on the bottom of the ice continued until the end of

Table 5. Comparison of HOTRAX Area Fractions and Estimated Areally Averaged Albedo to Results From SHEBA, National Technical Means (NTM), and AOS^a

Experiment	Date	Latitude	Longitude	Lead	Ice	Pond	Albedo
HOTRAX	22 Aug 2005	81°14'N	177°12'W	0.07	0.64	0.29	0.49
SHEBA	22 Aug 1998	78°16'N	165°56'W	0.18	0.80	0.02	0.54
NTM	21 Aug 1995	78°N	145°W	0.03	0.83	0.14	0.58
AOS	31 Jul 1994	76°02'N	171°44'W	0.06	0.82	0.12	0.57

^aSHEBA results from Perovich *et al.* [2002a], National Technical Means (NTM) results from Fetterer and Untersteiner [1998], and AOS results from Perovich and Tucker [1997].

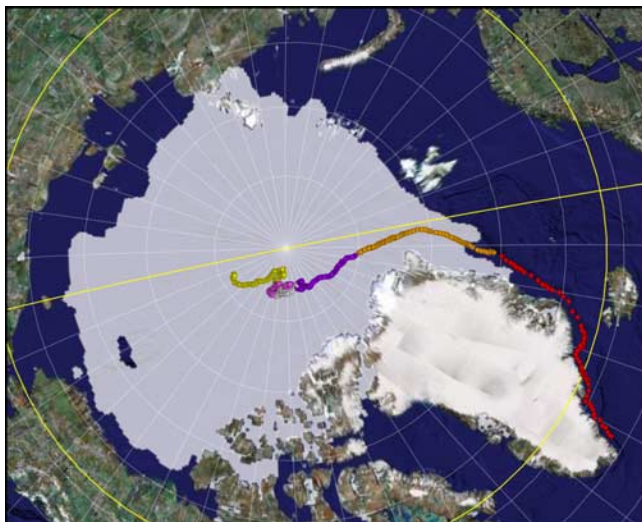


Figure 12. Results from an ice mass balance buoy installed at $85^{\circ}7.337'N$, $154^{\circ}47.979'W$ on 2 September 2005. (a) The drift track of the buoy is divided by season (yellow, fall 2005; magenta, winter 2006; white, spring 2006; purple, summer 2006; orange, fall 2006; red, winter 2007). The light blue shaded area denotes the ice extent in September 2006. Map courtesy of Google Earth and the National Snow and Ice Data Center [Fetterer *et al.*, 2008]. Google Earth imagery © Google Inc. Used with permission. (b) Time series from September 2005 to March 2007 of barometric pressure, air temperature, snow depth, ice growth, surface melt, bottom melt, and internal ice temperature. Also shown is the internal ice temperature using color contours, with blue being cold and red being warm. The gray shaded area represents snow depth, black areas are missing data, and the dark blue represents the ocean.

November 2006, with a total loss of only 0.13 m. There was little bottom growth during the second winter. During the last few days of the buoy, the ice floe entered relatively warm water and there was rapid bottom ablation of up to 0.1 m d^{-1} . In general, both growth and melt were modest on this thick multiyear ice floe.

4. Conclusions

[40] These observations illustrate the significant variability of ice morphology found across the Arctic basin. In the western Beaufort Sea, we observed extensive areas of undeformed first year ice with thickness 0.5–1 m. The ice concentration averaged about 0.7 and there was an abundance of surface melt ponds (areal fractions peaked at 0.5 and averaged 0.25). At $78^{\circ}N$ there was a shift from first year ice to multiyear ice, with bands of first year ice occasionally encountered during an east to west excursion. Once the cruise reached $79^{\circ}N$, multiyear ice became dominant and ice concentrations typically ranged from 0.8 to 1.0.

[41] The basin-wide ice thickness distribution had a mean thickness of 1.79 m. Approximately half of the ice was between 1 and 2 m thick, with another third between 2 and 3 m. There was a general latitudinal trend of increasing ice

thickness moving northward. However, there were exceptions to this general trend. Near the North Pole (longitudes $150^{\circ}E$ to $170^{\circ}E$) we traversed over 100 km of open water, nilas, and thin ice. Just beyond the pole heading south at 50 – $70^{\circ}E$ from $89^{\circ}22'N$ to $86^{\circ}39'N$, there was a region of very thick, massive floes where much of the ice was over 6 m thick (Sites 24, 26, and 28). This variability demonstrates that the ice cover is far from uniform.

[42] Details of how the Arctic ice pack responds to changes in forcing are not completely understood. Metrics such as reduced ice thickness and reduced ice extent reveal that there have been recent changes in the ice cover, but scientific consensus on the mechanisms by which these changes are occurring is lacking. Ice properties and processes that occur on scales smaller than can be remotely sensed, and oftentimes, smaller than are typically simulated in numerical climate models may offer clues to the fundamental nature of the observed large-scale changes in the ice cover.

[43] The advantage of making observations of sea ice morphology during a basin-wide transect such as HOTRAX lies in the ability to sample not only large-scale properties of the ice cover (e.g., thickness distributions, ice concentrations), but also to simultaneously sample smaller-scale properties. In particular, the observations of melt pond coverage and details of the ice crystallography that were made during this cruise may provide insight into the physics of widely observed large-scale changes.

[44] Extensive ponding was observed during the August portion of the cruise. The largest pond fractions were observed on first year ice, where the ice was flat and featureless with very little surface topography. Some of these ponds had melted through to the ocean. The melt season was long and did not finish until the end of August when the cruise reached latitude $84^{\circ}N$.

[45] Other than the creation of open ocean, surface melt ponds are the primary mechanism by which the albedo of the ice is reduced in summer. Given the large difference in albedo of bare ice in comparison to ponded ice, observations of the fractional coverage of ponded ice were used to estimate areally averaged albedos. Corresponding estimates of aggregate albedo carried out for SHEBA data and HOTRAX data showed that on 22 August, the albedo at SHEBA was 0.54, whereas on the same day, 7 years later, 330 km further north, the HOTRAX ponds had not yet started to freeze, and the large pond fraction resulted in a small areally averaged albedo (0.49). This demonstrates the importance of pond fraction on large-scale albedo.

[46] The average bulk salinity of all the cores was 1.6 ppt and values for individual cores ranged from 1.0 to 2.2 ppt. Five of the 12 cores contained ice that was more than 50% granular, an exceptionally large portion for multiyear Arctic sea ice. Older observations elsewhere in the Arctic place the granular fraction near 10%. Our observations indicate a granular ice fraction, of just over 40% averaged for the entire basin implying an increase of ice growth under turbulent conditions. Details of the interactions between ice type (granular/congelation), topography, age, salinity, ponding, and large-scale dynamics and ice-albedo feedback are not well understood, but these are inextricably linked to large-scale properties

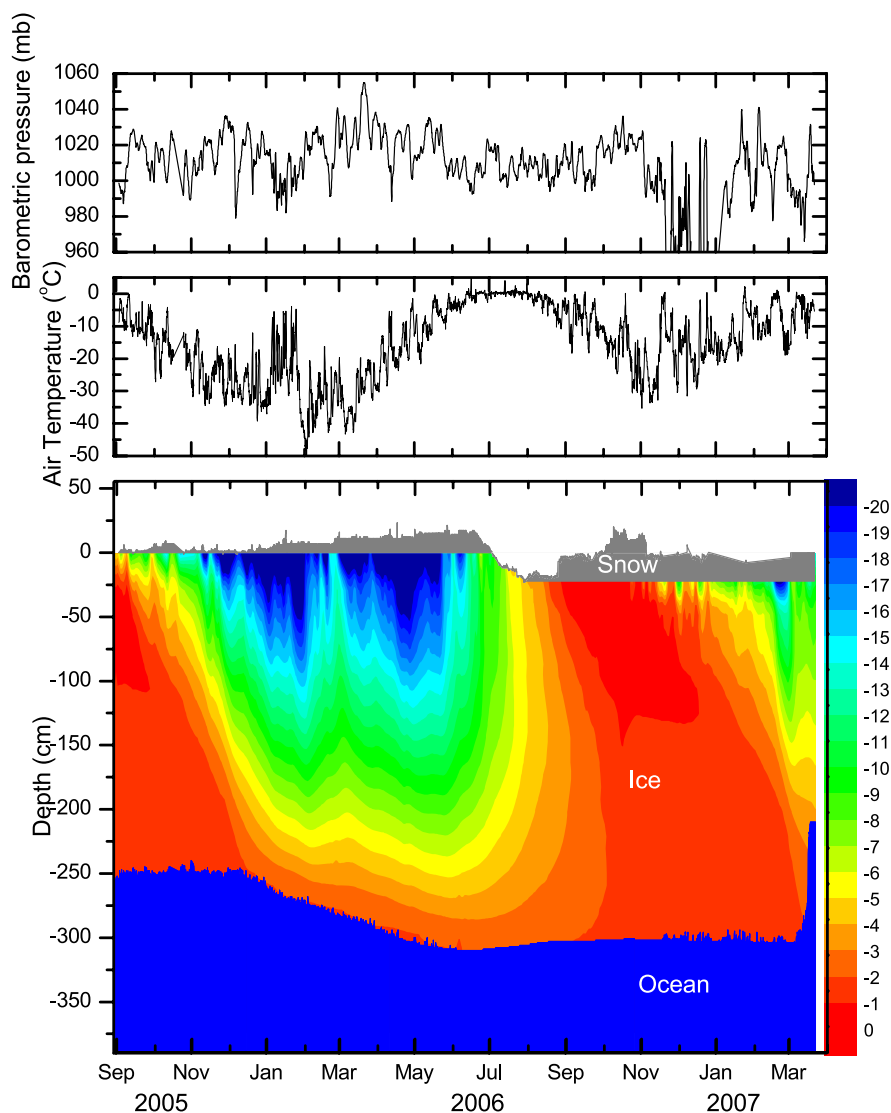


Figure 12. (continued)

(e.g., ice thickness, extent, area) that determine the well being of the sea ice cover.

[47] **Acknowledgments.** The authors thank the crew of the USCGC icebreaker *Healy* for their indefatigable assistance during the cruise. This work was funded by the National Science Foundation, Office of Polar Programs, Arctic Natural Sciences.

References

- Cavaliere, D. J., P. Gloersen, C. L. Parkinson, J. C. Comiso, and H. J. Zwally (1997), Observed hemispheric asymmetry in global sea ice changes, *Science*, *278*, 1104–1106, doi:10.1126/science.278.5340.1104.
- Clarke, A. D., and K. J. Noone (1985), Soot in the Arctic snowpack: A cause for perturbations in radiative transfer, *Atmos. Environ.*, *19*, 2045–2053, doi:10.1016/0004-6981(85)90113-1.
- Comiso, J. C. (2002), A rapidly declining perennial sea ice cover in the Arctic, *Geophys. Res. Lett.*, *29*(20), 1956, doi:10.1029/2002GL015650.
- Comiso, J. C., C. L. Parkinson, R. Gersten, and L. Stock (2008), Accelerated decline in the Arctic sea ice cover, *Geophys. Res. Lett.*, *35*, L01703, doi:10.1029/2007GL031972.
- Darby, D. A., M. Jakobsson, and L. Polyak (2005), Icebreaker expedition collects key Arctic seafloor and ice data, *Eos Trans. AGU*, *86*(52), doi:10.1029/2005EO520001.
- Eicken, H., M. Lensu, M. Leppäranta, W. B. Tucker III, A. J. Gow, and O. Salmela (1995), Thickness, structure, and properties of level summer multiyear ice in the Eurasian sector of the Arctic Ocean, *J. Geophys. Res.*, *100*, 22,697–22,710, doi:10.1029/95JC02188.
- Eicken, H., W. B. Tucker III, and D. K. Perovich (2001), Indirect measurements of the mass balance of summer Arctic sea ice with an electromagnetic induction technique, *Ann. Glaciol.*, *33*, 194–200, doi:10.3189/172756401781818356.
- Fetterer, F., and N. Untersteiner (1998), Observations of melt ponds on Arctic sea ice, *J. Geophys. Res.*, *103*, 24,821–24,835.
- Fetterer, F., K. Knowles, W. Meier, and M. Savoie (2008), Sea ice index, Natl. Snow and Ice Data Cent., Boulder, Colo., www.nsidc.org/data/seaiice_index.
- Gow, A. J., and W. B. Tucker III (1987), Physical properties of sea ice discharged from Fram Strait, *Science*, *236*, 436–439.
- Grenfell, T. C., and D. K. Perovich (2004), The seasonal and spatial evolution of albedo in a snow-ice-land-ocean environment, *J. Geophys. Res.*, *109*, C01001, doi:10.1029/2003JC001866.
- Grenfell, T. C., B. Light, and M. Sturm (2002), Spatial distribution and radiative effects of soot in the snow and sea ice during the SHEBA experiment, *J. Geophys. Res.*, *107*(C10), 8032, doi:10.1029/2000JC000414.
- Haas, C. (2004), Late-summer sea ice thickness variability in the Arctic Transpolar Drift 1991–2001 derived from ground-based electromagnetic sounding, *Geophys. Res. Lett.*, *31*, L09402, doi:10.1029/2003GL019394.
- Haas, C., and H. Eicken (2001), Interannual variability of summer sea ice thickness in the Siberian and central Arctic under different atmospheric circulation regimes, *J. Geophys. Res.*, *106*, 4449–4462, doi:10.1029/1999JC000088.

- Haas, C., S. Gerland, H. Eicken, and H. Miller (1997), Comparison of sea ice thickness measurements under summer and winter conditions in the Arctic using a small electromagnetic induction device, *Geophysics*, *62*, 749–757, doi:10.1190/1.1444184.
- Inoue, J., T. Kikuchi, and D. Perovich (2008), Effect of heat transmission through melt ponds and ice on melting during summer in the Arctic, *J. Geophys. Res.*, *113*, C05020, doi:10.1029/2007JC004182.
- Johannessen, O. M., M. Miles, and E. Bjorgo (1995), The Arctic shrinking sea ice, *Nature*, *376*, 126–127, doi:10.1038/376126a0.
- Kwok, R. (2007), Near zero replenishment of the Arctic multiyear sea ice cover at the end of 2005 summer, *Geophys. Res. Lett.*, *34*, L05501, doi:10.1029/2006GL028737.
- Light, B., T. C. Grenfell, and D. K. Perovich (2008), Transmission and absorption of solar radiation by Arctic sea ice during the melt season, *J. Geophys. Res.*, *113*, C03023, doi:10.1029/2006JC003977.
- Meese, D. A. (1989), The chemical and structural properties of sea ice in the southern Beaufort Sea, *Rep. 89-25*, Cold Reg. Res. Eng. Lab., Hanover, N.H.
- Nghiem, S. V., Y. Chao, G. Neumann, P. Li, D. K. Perovich, T. Street, and P. Clemente-Colón (2006), Depletion of perennial sea ice in the eastern Arctic Ocean, *Geophys. Res. Lett.*, *33*, L17501, doi:10.1029/2006GL027198.
- Nghiem, S. V., I. G. Rigor, D. K. Perovich, P. Clemente-Colón, J. W. Weatherly, and G. Neumann (2007), Rapid reduction of Arctic perennial sea ice, *Geophys. Res. Lett.*, *34*, L19504, doi:10.1029/2007GL031138.
- Parkinson, C. L., D. J. Cavalieri, P. Gloersen, H. J. Zwally, and J. C. Comiso (1999), Arctic sea ice extents, areas, and trends 1978–1996, *J. Geophys. Res.*, *104*, 20,837–20,856, doi:10.1029/1999JC900082.
- Pegau, W. S., and C. A. Paulson (2001), The albedo of Arctic leads in summer, *Ann. Glaciol.*, *33*, 221–224, doi:10.3189/172756401781818833.
- Perovich, D. K., and J. A. Richter-Menge (2006), From points to poles: Extrapolating point measurements of sea ice mass balance, *Ann. Glaciol.*, *44*, 188–192, doi:10.3189/172756406781811204.
- Perovich, D. K., and W. B. Tucker III (1997), Arctic sea ice conditions and the distribution of solar radiation during summer, *Ann. Glaciol.*, *25*, 445–450.
- Perovich, D. K., W. B. Tucker III, and K. A. Ligett (2002a), Aerial observations of the evolution of ice surface conditions during summer, *J. Geophys. Res.*, *107*(C10), 8048, doi:10.1029/2000JC000449.
- Perovich, D. K., T. C. Grenfell, B. Light, and P. V. Hobbs (2002b), Seasonal evolution of the albedo of multiyear Arctic sea ice, *J. Geophys. Res.*, *107*(C10), 8044, doi:10.1029/2000JC000438.
- Perovich, D. K., T. C. Grenfell, J. A. Richter-Menge, B. Light, W. B. Tucker III, and H. Eicken (2003), Thin and thinner: Sea ice mass balance measurements during SHEBA, *J. Geophys. Res.*, *108*(C3), 8050, doi:10.1029/2001JC001079.
- Richter-Menge, J. A., D. K. Perovich, B. C. Elder, I. Rigor, and M. Ortmeier (2006), Ice mass balance buoys: A tool for measuring and attributing changes in the thickness of the Arctic sea ice cover, *Ann. Glaciol.*, *44*, 205–210, doi:10.3189/172756406781811727.
- Rigor, I., and J. M. Wallace (2004), Variations in the age of Arctic sea ice and summer sea ice extent, *Geophys. Res. Lett.*, *31*, L09401, doi:10.1029/2004GL019492.
- Rind, D., R. Healy, C. Parkinson, and D. Martinson (1995), The role of sea ice in $2 \times \text{CO}_2$ climate model sensitivity. Part I: The total influence of sea ice thickness and extent, *J. Clim.*, *8*, 450–463.
- Rothrock, D. A., Y. Yu, and G. A. Maykut (1999), Thinning of the Arctic sea ice cover, *Geophys. Res. Lett.*, *26*, 3469–3472, doi:10.1029/1999GL010863.
- Serreze, M. C., A. P. Barrett, A. G. Slater, M. Steele, J. Zhang, and K. E. Trenberth (2007), The large-scale energy budget of the Arctic, *J. Geophys. Res.*, *112*, D11122, doi:10.1029/2006JD008230.
- Stroeve, J., M. C. Serreze, F. Fetterer, T. Arbetter, W. Meier, J. Maslanik, and K. Knowles (2005), Tracking the Arctic's shrinking ice cover: Another extreme September minimum in 2004, *Geophys. Res. Lett.*, *32*, L04501, doi:10.1029/2004GL021810.
- Stroeve, J., M. M. Holland, W. Meier, T. Scambos, and M. Serreze (2007), Arctic sea ice decline: Faster than forecast, *Geophys. Res. Lett.*, *34*, L09501, doi:10.1029/2007GL029703.
- Tucker, W., and D. Cate (Eds.) (1996), The 1994 Arctic Ocean section, the first major scientific crossing of the Arctic Ocean, *Rep. A952223*, 117 pp., Cold Reg. Res. Eng. Lab., Hanover, N.H.
- Tucker, W. B., III, A. J. Gow, and W. F. Weeks (1987), Physical properties of summer sea ice in the Fram Strait, *J. Geophys. Res.*, *92*, 6787–6803, doi:10.1029/JC092iC07p06787.
- Tucker, W. B., III, A. J. Gow, D. A. Meese, H. W. Bosworth, and E. Reimnitz (1999), Physical characteristics of summer sea ice across the Arctic Ocean, *J. Geophys. Res.*, *104*, 1489–1504, doi:10.1029/98JC02607.
- Tucker, W. B., III, J. W. Weatherly, D. T. Eppler, D. Farmer, and D. L. Bentley (2001), Evidence for the rapid thinning of sea ice in the western Arctic Ocean at the end of the 1980s, *Geophys. Res. Lett.*, *28*, 2851–2854, doi:10.1029/2001GL012967.
- Untersteiner, N. (1961), On the mass and heat budget of Arctic sea ice, *Arch. Meteorol. Geophys. Bioklimatol., Ser. A*, *12*, 151–182, doi:10.1007/BF02247491.
- Warren, S. G., and A. D. Clarke (1990), Soot in the atmosphere and snow surface of Antarctica, *J. Geophys. Res.*, *95*, 1811–1816, doi:10.1029/JD095iD02p01811.
- Warren, S. G., and W. J. Wiscombe (1980), A model for the spectral albedo of snow. II: Snow containing atmospheric aerosols, *J. Atmos. Sci.*, *37*, 2734–2745.
- Worby, A. P. (1999), Observing Antarctic sea ice: A practical guide for conducting sea ice observations from vessels, report, Sci. Comm. for Antarct. Res., Hobart, Tasmania.

B. C. Elder and D. K. Perovich, CRREL, ERDC, 72 Lyme Road, Hanover, NH 03755, USA. (donald.k.perovich@erdc.usace.army.mil)

T. C. Grenfell, Department of Atmospheric Sciences, University of Washington, Seattle, WA 98195, USA.

J. Harbeck, Geophysical Institute, University of Alaska Fairbanks, Fairbanks, AK 99775, USA.

B. Light, Polar Science Center, University of Washington, Seattle, WA 98125, USA.

C. Polashenski and C. Stelmach, Thayer School of Engineering, Dartmouth College, Hanover, NH 03755, USA.

W. B. Tucker III, Terry Tucker Research, 432 Methodist Hill Road, Enfield, NH 03748, USA.